Earth and Planetary Science Letters 287 (2009) 345–352

Contents lists available at ScienceDirect

Earth and Planetary Science Letters

journal homepage: www.elsevier.com/locate/epsl

Single-crystal elasticity of $(Mg_{0.9}Fe_{0.1})O$ to 81 GPa

Hauke Marquardt [a,*], Sergio Speziale [a], Hans J. Reichmann [a], Daniel J. Frost [b], Frank R. Schilling [a,1]

[a] GFZ German Research Centre for Geosciences, Telegrafenberg, 14473 Potsdam, Germany
[b] Bayerisches Geoinstitut, Universität Bayreuth, 95440 Bayreuth, Germany

ARTICLE INFO

Article history:
Received 8 May 2009
Received in revised form 7 August 2009
Accepted 11 August 2009
Available online 19 September 2009

Editor: R.D. van der Hilst

Keywords:
spin transition
ferropericlase
elastic properties
Brillouin
high-pressure

ABSTRACT

Ferropericlase is the second most abundant mineral in Earth's lower mantle and knowledge of its elastic properties at relevant conditions is needed to adequately interpret seismic observations in terms of the mineralogy and thermal state of the deep Earth. Here, we report the complete elastic tensor of $(Mg_{0.9}Fe_{0.1})O$ ferropericlase to 81.2 GPa at room temperature measured by Brillouin spectroscopy and X-ray diffraction in the diamond-anvil cell. Our data indicate that the spin transition of iron between 45 and 63 GPa dramatically affects the longitudinal and off-diagonal elements of the elastic stiffness tensor c_{11} and c_{12}, whereas it leaves the shear constant c_{44} almost unaffected. Based on our results, the spin transition markedly changes the pressure (and temperature) dependence of the compressional and bulk sound velocities and must be taken into account in any attempt to match average radial seismic velocity profiles with mineral physics observations. The different pressure dependence of compressional (and bulk) and shear sound velocities across the high-spin to low-spin (HS–LS) transition implies that the spin transition might be best observed in the v_p/v_s ratio and its pressure (and temperature) derivative. We also point out the possibility that the spin transition leads to an anti-correlated temperature dependence of shear and compressional wave speeds in certain pressure–temperature regimes in Earth's lower mantle.

1. Introduction

To date, the most complete picture of the structure, evolution and present-day dynamics of the Earth's lower mantle emerges from the interpretation of seismological observations. An interpretation of seismic wave velocities in terms of mineralogy and temperature requires detailed knowledge of the physical properties of candidate phases at pressure (P)–temperature (T) conditions relevant to the Earth's deep interior. It is commonly assumed that ferropericlase with a composition of approximately $(Mg_{0.8}Fe_{0.2})O$ is the second most abundant mineral (~20 vol.%) of Earth's lower mantle (Bina et al., 2003, Lee et al., 2004). Understanding its elastic properties as a function of iron content and iron spin state is thus a major challenge. Previous studies of the elasticity of (Mg,Fe)O have shown that the shear modulus is much more sensitive to iron content than the bulk modulus (at least for Mg-rich ferropericlase in high-spin state) (Jackson et al., 1978, Bonczar and Graham, 1982, Jacobsen et al., 2002, Jackson et al., 2006). This emphasizes the importance of quantifying the elastic shear properties in order to distinguish different compositional models for the lower mantle (Kung et al., 2002).

Recently, it has been shown by a number of different experimental techniques that Fe^{2+} in ferropericlase changes its electronic configuration at pressures corresponding to Earth's lower mantle (e.g. Badro et al., 2003, Lin et al., 2005, Speziale et al., 2005, Goncharov et al., 2006, Lin et al., 2007). The high-spin (HS) to low-spin (LS) transition involves a pairing of the 3d-electrons in the energetically favoured t_{2g}-orbitals. Iron in LS configuration has a smaller ionic radius than its HS counterpart [LS Fe^{2+}: 0.61–0.72 Å (Shannon, 1976, Fei et al., 2007), HS Fe^{2+}: 0.78 Å (Shannon, 1976)] and the spin transition is accompanied by a volume change of the host mineral (Lin et al., 2005, Tsuchiya et al., 2006, Fei et al., 2007, Speziale et al., 2007, Stackhouse et al., 2007). It has also been shown that the iron spin transition affects sound wave propagation characteristics of (Mg,Fe)O (Lin et al., 2006, Crowhurst et al., 2008, Marquardt et al., 2009), but the implications for the interpretation of seismic observations are still under debate. From our current knowledge, the magnitude of the effects on the elastic properties associated with the HS–LS transition are stronger for the simple oxide ferropericlase than for the co-existing $(Mg,Fe)SiO_3$ phases, because the oxide contains more iron, most of the iron is ferrous, and all iron is in octahedral coordination (Lundin et al., 2008). We present the elastic constants of $(Mg_{0.9}Fe_{0.1})O$ measured by Brillouin scattering and X-ray diffraction in a diamond-anvil cell to 81.2 GPa and show that the HS–LS transition has visible effects on the longitudinal and off-diagonal elastic stiffness constants, but does not clearly affect the shear constants. This mechanism leads to considerable changes in the pressure and temperature derivatives of the compressional and bulk sound velocity. The spin transition could even cause an anti-correlated temperature dependence of bulk (and possibly compressional) and shear wave velocities in Earth's lower mantle. These findings have significant effects on the thermochemical

* Corresponding author.
E-mail address: hama@gfz-potsdam.de (H. Marquardt).
[1] Present address: Karlsruhe Institute of Technology, IAG, 76131 Karlsruhe, Germany.

0012-821X/$ – see front matter © 2009 Elsevier B.V. All rights reserved.
doi:10.1016/j.epsl.2009.08.017

interpretations of the lower mantle (paper in preparation) and should be considered for both one-dimensional seismic models and seismic tomography images of lateral heterogeneity in Earth's lower mantle (e.g. Su and Dziewonski, 1997, Kennett et al., 1998, Masters et al., 2000, Karato and Karki, 2001, Romanowicz, 2003, Kennett and Gorbatov, 2004, Saltzer et al., 2004, Cammarano et al., 2005, Mattern et al., 2005).

2. Materials and methods

2.1. Sample material

Single-crystal ferropericlase was synthesised from a powder in a multi-anvil apparatus at *P–T*-conditions corresponding to Earth's lower mantle (24 GPa, 1800 °C). The annealing procedure ensured a ferric iron content below the detection limit of Mößbauer Spectroscopy, as previously documented for ferropericlase synthesised in the same laboratory with the same method (Keppler et al., 2007). The resulting crystals were slightly greenish crystals with a diameter of up to 100 µm. Details of the synthesis have been reported elsewhere (Marquardt et al., 2009). Microprobe analyses yielded a composition of $(Mg_{0.900(3)}Fe_{0.100(3)})O$ and indicated compositional homogeneity.

2.2. X-ray diffraction

Single-crystal X-ray diffraction at room pressure was performed at the Bayerisches Geoinstitut using molybdenum as an X-ray emitting source. Crystals from the same synthesis were crushed between diamonds to produce a powder, which was loaded in symmetric piston-cylinder diamond anvil cells (Mao et al., 1997) for high-pressure synchrotron X-ray diffraction measurements at beamline I15 of Diamond Light Source, UK. The experiments were performed in two different runs up to 77 GPa (Fig. 1) using diamonds with 300 µm culets and rhenium as the gasket material. Neon was employed as the pressure-transmitting medium and the pressure was determined by ruby fluorescence from at least two ruby spheres before and after each X-ray diffraction measurement. Sample detector distance and energy (28 keV) of the incoming beam were calibrated using a silicon standard. Diffraction images were collected on a MAR 345 image plate. The fit2d program (Hammersley et al., 1996, Hammersley, 1997, Hammersley, 1998) was used to convert the images into 2-dimensional diffraction patterns and the peak positions were fitted using peak fit software. The unit cell volume V was determined based on three diffraction peaks corresponding to the (200), (111) and (220) lattice planes.

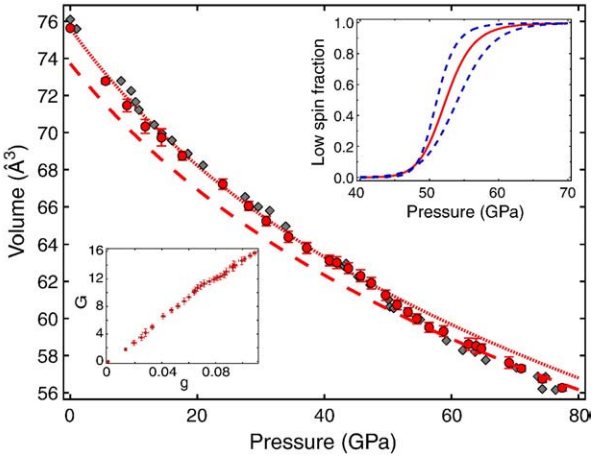

Fig. 1. Isothermal compression curve of $(Mg_{0.9}Fe_{0.1})O$. The red dotted and dashed lines represent the extrapolation of the HS and LS phase, respectively. The grey diamonds show results for $(Mg_{0.83}Fe_{0.17})O$ (Lin et al., 2005) for comparison. The anomalous compression behaviour is also clearly visible in the *G–g* plot (inset in the lower left corner), where $g = 0.5\cdot[(V_0^{HS}/V)^{2/3} - 1)]$ and $G = g\cdot[P/(3g(1+2g)^{5/2}]$ (Jeanloz, 1981). The inset in the upper right corner shows the pressure dependence of the fraction of LS Fe^{2+} in $(Mg_{0.9}Fe_{0.1})O$, where the solid red line represents the average values and the upper and lower bounds are illustrated as blue dashed lines. (For interpretation of the references to colour in this figure legend, the reader is referred to the web version of this article.)

The $V(P)$ data were separated into two pressure ranges for the HS (to 45 GPa) and LS (from 63 GPa) phases and over each range the volumes were fitted to a third order Birch–Murnaghan equation of state (Fig. 1, details below). The thermodynamic relations $K_{0T} = K_{0S}/(1+\alpha_0\gamma_0 T)$ and $(\partial K_{0T}/\partial P)_T \cong (1+\alpha_0\gamma_0 T)^{-1}$ $[(\partial K_{0S}/\partial P)_T - \gamma_0 T/K_T (\partial K_{0T}/\partial T)_P]$ where the index 0 indicates ambient conditions (Speziale and Duffy, 2002) were employed to obtain K_{0S} and K_{0S}' for the LS phase. The volumetric thermal expansion and the Grüneisen parameter at ambient conditions $\alpha_0 = 31.2\cdot10^{-6}\ K^{-1}$ and $\gamma_0 = 1.524$ were assumed to be the same as for MgO (taken from Suzuki, 1975 and Speziale et al., 2001). Note that even if both α_0 and γ_0 differed by 20% for $(Mg_{0.9}Fe_{0.1})O$ compared to MgO, the resulting difference in adiabatic bulk modulus would be less than 1%. Eulerian finite-strain equations (Davies and Dziewonski, 1975, Karki et al., 2001) were used to calculate the adiabatic bulk modulus $K_s = (c_{11} + 2c_{12})/3$ at high-pressures to complement the Brillouin scattering results (see Section 2.3).

2.3. Brillouin scattering

High-pressure Brillouin scattering experiments were performed on three different single-crystal platelets from the same synthesis experiment. 45–80 µm-sized crystals were double-side polished to a thickness of between 18 and 30 µm for high-pressure Brillouin scattering experiments. In three independent experimental runs, the platelets were loaded together with different pressure-transmitting-media (methanol:ethanol:water (MEW) 16:3:1 volume ratio, argon, or neon) in diamond-anvil-cells with culet sizes of either 300 or 500 µm (Table 1). Argon loading was performed cryogenically at GFZ Potsdam, whereas the gas-loading facility at Bayerisches Geoinstitut was used to load neon with a pre-pressure of 1.5 kbar. Along with the sample, annealed ruby spheres were loaded as a pressure calibrant in the sample chamber. Either stainless steel or rhenium was used as gasketing material. Brillouin scattering experiments were performed in symmetric 60° or 80°-forward scattering geometry up to a maximum pressure of 81.2 GPa. The sample platelets were rotated around the axis perpendicular to their faces and velocities were measured in different crystallographic directions in the platelets plane. An inversion procedure (Every, 1980) based on Christoffel's equation was used to determine the elastic constants and refine the orientation of the sample (e.g. Shimizu and Sasaki, 1992), which turned out to be (001) in all experimental runs. At pressures above 32 GPa, the Brillouin signal corresponding to the longitudinal wave was masked by inelastic scattering from the diamond shear waves. However, probing the shear velocities in different crystallographic directions in the (100) plane (Fig. 2) allowed us to determine the two elastic shear constants c_{44} and $c_s = (c_{11} - c_{12})/2$. At each pressure above 32 GPa, the Brillouin elasticity data were combined with the (adiabatic) bulk modulus calculated from the EoS parameters derived from X-ray powder diffraction. The elastic stiffness constants c_{11} and c_{12} were then calculated from c_s and K_s using the identities

Table 1
Experimental conditions for Brillouin scattering experiments.

Run	Sample diameter	Sample thickness	Culet size	Gasket material	Pressure medium	Max. pressure
1	80 µm	30 µm	500 µm	Steel	MEW	17.0 GPa
2	60 µm	25 µm	500 µm	Steel	Argon	31.6 GPa
3	45 µm	18 µm	300 µm	Rhenium	Neon	81.2 GPa